The effect of iron and the precipitation behavior of iron during annealing of a cold deformed commercial purity aluminium alloy

Sindre Bunkholt[a], Erik Nes[b], Knut Marthinsen[b]

[a]Hydro Aluminium Rolled Products AS, Weidemanns gate 8, N-3080 Holmestrand, Norway

[b] Department of Materials Science and Engineering, Norwegian University of Science and Technology (NTNU), Alfred Getz vei 2, N-7491 Trondheim, Norway

*Corresponding author: Prof. Knut Marthinsen; Tel.: +47 73593473; fax: +47 73550203.
E-mail address: knut.marthinsen@ntnu.no

Abstract

Iron is always present in any aluminium alloy and usually as an impurity element. In commercial purity alloys the concentration of iron is typically so large that iron has a strong influence on the material properties, due to its slow diffusivity and low solubility in aluminium. In the present work the effect of iron in solid solution and the precipitation behavior of iron during annealing of a cold-deformed commercial purity aluminium alloy have been investigated. Iron in solution is found to have a strong retarding effect on the softening kinetics. The resulting recrystallization texture has a distinct Cube component and some weak deformation texture components. By additional cold rolling and inter-annealing, the solute content is reduced significantly by precipitation of mainly Al_3Fe and some α-AlFeSi phases. Doing so speeds up the softening kinetics by a factor of ~1000 and causes a considerable strengthening of the Cube component in the recrystallized texture.

Keywords: Aluminium, Softening, Inter-annealing, Precipitation, Texture.

1. Introduction

Alloy elements are typically associated with elements that are added on purpose in order to achieve some specific properties. Iron is always present in all aluminium alloys and is regarded as the main impurity element, although it can also be added on purpose to high purity alloys in order to improve strength [1]. Iron is introduced during production and preparation of aluminium castings, where iron will get in contact with the melt and some iron will be dissolved by aluminium. However, the solubility of iron in aluminium is relatively low at all temperatures, and once present, iron in industrial alloys cannot be readily removed at a low cost [2]. Thus, iron is always present. Moreover, it will accumulate with recycling and, due to the low solubility, form large constituent phases that can be detrimental to the mechanical properties [1].

In most alloys the effect of iron impurities can be neglected because other elements have a stronger influence on the properties and the effects of iron are suppressed, e.g. by modifying the iron-rich constituent particles. On the other hand, in pure aluminium alloys iron is historically seen to have a strong effect on both mechanical properties and texture though its influence on annealing behavior [3,4]. Both commercial and high purity alloys with an iron content of less than 100 ppm may be greatly influenced by inter-annealing processes that alter the level of dissolved iron. Marshall et al. [5] investigated the annealing response of a 99.5% pure alloy after cold rolling and found inter-annealing at temperatures $\leq$ 400 °C to significantly promote softening. The authors proposed dissolution of Al_3Fe and AlFeSi particles, formed during homogenization, during high temperature inter-annealing which resulted in a strong solute drag effect that retarded recovery and recrystallization in subsequent annealing processes. On the other hand, Hasenclever [6] has confirmed a reduction of the solute level of iron after final annealing in commercial purity aluminium with inter-annealing. Actually, there is strong evidence for a redistribution of dissolved

iron into precipitates in both high and commercial purity aluminium alloys in the literature [7-11]. Preferential clustering or precipitation of iron is taking place on lattice defects in high purity alloys containing as little as 2 ppm iron during annealing [12]. The precipitating phases are typically Al_6Fe, Al_3Fe and possibly AlFeSi if small amounts of Si also are present.

Because of the strong drag effect exerted on dislocations and subgrain boundaries by dissolved iron, precipitation not only influences the rate of recovery but also the resulting recrystallization texture. Marshall and Ricks [4] found that increasing levels of iron in solution during annealing impeded the formation of the Cube texture component. Ito et al. [13,14] made similar findings and also found that the R texture component was promoted by iron in solution. Since both Cube- and R-grains grow by motion of 40° <111> boundaries, the authors believed it was the nucleation mechanism that was influenced by iron in and out of solution. Ito et al. [13] found that if precipitation took place before recrystallization, the Cube texture component would be suppressed due to the Zener drag from precipitates affecting boundary motion. However, Suzuki et al. [15] found the opposite to be true, i.e. that in a matrix with nearly complete precipitation of iron, the Cube texture component easily develops during recrystallization. Ekström et al. [16] found that removing iron from solution in commercial purity alloys strengthened the Cube component and, rather surprisingly, that the strongest Cube texture was detected in a sample designed to have high solute level of iron.

Literature gives an in depth view of how high and commercial purity alloys may be affected by iron, although the above observations illustrate that the effect of iron may be difficult to predict and appear at times rather case-specific [3-6,13,14]. The precipitation kinetics and recovery mechanisms are very dependent on accurate solute measurements, the processing route (homogenization, inter-annealing etc.) and processing parameters (temperatures, heating rates

etc.). Often the investigations are designed in order to study a particular feature or mechanism and there are few works that study recovery kinetics, precipitation and recrystallization texture simultaneously. The present work aims to describe the effect of iron in a commercial AA1070 alloy experiencing different process routes mimicking those seen industrially, especially without and with inter-annealing during cold rolling and final annealing. The aim is to tie together several effects related to iron by using a fairly standard material (commercial purity alloy) and linking it to literature observations [4,10,11,13,14,17].

2. Experimental

In industrial rolling, an alloy is typically delivered to the customer in cold rolled or annealed state depending on the desired properties. Irrespective of the final state, it can also be necessary to inter-anneal the material. For commercial purity materials, that means that the behavior of iron has to be well known. In this study a commercial AA1070 alloy was used where the rolling slabs were cut from a DC cast billet. The alloy contained 0.15 wt.% Fe and 0.07 wt.% Si and the homogenization scheme was intended to create high levels of dissolved iron. The slabs were homogenized at a temperature of 620 °C and held there for 6 hours before water quenching, in order to maximize the amount of iron in solid solution before further processing.

The slabs were subsequently cold rolled with lubricated rolls in several passes down to a reduction of 50% (ε=0.7) and 92.5% (ε=2.6). Some of the 50% and 92.5% deformed material was fully soft-annealed at 320 °C and 300 °C, respectively. The 50% deformed and inter-annealed material was further deformed another 50% and 92.5%, while the 92.5% and inter-annealed material was only deformed another 50%. This processing resulted in 5 different sample states according to Table 1. The samples with 50% final deformation were annealed at 320 °C, while

those with a final deformation of 92.5% were annealed at 300 °C. All samples where annealed for time increments up to 10^5 seconds. These special processing routes were designed to highlight iron precipitation characteristics during annealing and the effects of iron in solid solution on the softening behavior after different degrees of deformation, with and without inter-annealing, during cold rolling and final annealing.

Electrical conductivity measurements were used to estimate the solute level before and after homogenization and in cold rolled and annealed samples. Only the measurements performed by a Sigmascope EX8 instrument are presented here but they were confirmed by resistivity ratio measurements by the four point method. The softening behavior was characterized by conductivity measurements in addition to Vickers hardness measurements and texture investigations of deformed and fully soft samples. The texture was measured by EBSD in a Hitachi SU6600 FE-SEM with EDAX TSL OIM Analysis software and presented in the form of orientation distribution functions (ODF). Sample preparation for EBSD scanning was done by mechanical polishing and electrochemical polishing using a 10% perchloric acid ethanol solution. The distribution of iron-rich precipitates was investigated by etching samples in a 5% HF solution for 30 seconds [8,17]. The precipitates in directly annealed samples were characterized by bright field imaging, selected area diffraction and energy dispersive spectroscopy (EDS) in a JEOL JEM-2010 transmission electron microscope (TEM) on samples electro polished using a 33% nitric acid methanol solution.

3. Results

In the as-cast condition the electrical conductivity measurement resulted in a conductivity of 34.9 m/Ωmm^2. After homogenization the conductivity dropped to 34.7 m/Ωmm^2. These measurements were confirmed by 4-point probe measurements conducted on the same materials

in Hydro Aluminium Rolled Products' R&D center at 4.2K, resulting in 35.01 m/Ωmm^2 and 34.36 m/Ωmm^2 in as-cast and homogenized state respectively. This result is indicating a weak increase in the level of dissolved iron during homogenization. Larger changes to the conductivity were expected and confirmed in the annealed samples, which evolution during final annealing is shown in Fig. 1. The softening behavior is shown by Vickers' hardness vs. annealing time in Fig. 2.

Firstly, it can be seen in Fig.1 that inter-annealing (B, C and E) significantly increases conductivity of the deformed samples. With more deformation before intermediate annealing, i.e. sample C, the conductivity increases further. The two samples that have experienced only 50% deformation in the first step, sample A and B, have similar conductivity after annealing for 10^5 seconds. For the samples with a final deformation of 92.5% (D and E) it can be seen that the conductivity actually increases more after annealing to fully soft condition if not inter-annealed (D). Of the 50% deformed samples (prior to final annealing) it is the sample with the highest conductivity, i.e. sample C that also shows the highest strength. However, this sample is also the least stable and softens completely within 10^3 seconds. Without inter-annealing, sample A have the lowest strength but is distinctively slower to soften than both the inter-annealed samples. Looking at the 92.5% deformed samples, the as-deformed hardness is similar, but also in this case the inter-annealed sample E softens faster. The inter-annealed samples recrystallize faster by about a factor 10^3. Comparing Fig.1 and Fig. 2, in the samples not inter-annealed (A and D), about 50% of the increase in conductivity takes place before the onset of recrystallization, i.e. at about 10^4 and 10^3 seconds for sample A and D, respectively, i.e. corresponding to where there are distinct changes in the slopes of the softening curves.

Etching of the polished surface of the annealed samples revealed significant pitting in all samples, indicating the presence of precipitates [12]. However, in as-deformed state and before

any inter-annealing no etch pits could be seen on the polished surfaces. TEM investigations of the same samples confirm that the as-deformed samples without any inter-annealing are free from precipitates. However, in the directly annealed samples two types of iron rich precipitates were identified. Type 1, shown in Fig. 3 was spherical, measuring from a few nanometers and up to 200 nm in diameter, and contained only iron according to in-situ EDS spectra. The majority of the precipitates were of this phase. Also in Fig 3, a larger and more elongated type 2 precipitate is shown. In-situ EDS revealed that this precipitate contained both iron and silicon. These precipitates were typically 20-50 nm wide and several hundred nanometers long. By means of selected area diffraction patterns from the two types of precipitates, the first one was identified as partially coherent Al_3Fe phase while the second type was found to be the α_h-AlFeSi phase where no coherency was detected [18,19].

The graphical presentation of texture is here limited to the annealing textures, although the texture after deformation was also recorded for all samples. 50% reduction was not enough deformation for the samples to develop a well-defined β-fiber texture. With inter-annealing the texture got much closer to the ideal β-fiber (in as-deformed state) although the peak intensity dropped, particularly in sample C with the most deformation before inter-annealing. The 92.5% deformed samples, on the other hand, both had a typical β-fiber texture with similar peak intensity, although the inter-annealed sample had stronger Brass and S components than sample D.

The resulting textures after annealing are summarized in Fig. 4 in form of ODFs (Euler space representation) showing only the constant $\varphi_2=0°$ section. For samples A and B, deformed only 50%, the textures are very weak. In sample C, which was deformed 92.5% before inter-annealing, 50% deformation followed by annealing resulted in a typical recrystallization texture with Cube and RD-rotated Cube components. There are no visible remains of the deformation

texture components. Sample D had very much the same texture as sample C. Sample E, which is similar to sample D but with inter-annealing, have a weak Brass component in addition to a stronger and more defined Cube component. There is also a weak S component when looking at the complete ODF. The most noticeable difference is the stronger Cube component and that the RD-rotated Cube and Goss components are replaced by a TD-rotated Cube component instead.

4. Discussion

The precipitation potential of iron is calculated to be about 300 ppm during annealing at 320 °C by Thermo-Calc (COST 507 dataset) when assuming prior homogenization at 620 °C. By applying Matthiessen's rule to the conductivities after annealing (35.8 m/Ωmm^2), presented in Fig. 1, we find that most of the 300 ppm dissolved iron have precipitated, i.e. all samples which have at some point been deformed 92.5% reach equilibrium after annealing. 300-320 °C is within the temperature range where the most precipitation takes place also according to literature[4,20]. After 50% deformation and annealing there is still more iron in solution than the equilibrium level at 320 °C. By more heavy deformation (92.5%) after inter-annealing the solute level is closer to equilibrium after the final annealing. However, most precipitation takes place when the samples is heavily deformed initially and then annealed. Further light deformation followed by annealing does not cause significantly more precipitation to take place as we see from the electrical conductivity measurements of sample C compared to samples D in Figure 1.

The above observations suggest that the dislocation and subgrain structure present in the microstructure after deformation is essential in order to relieve the matrix from dissolved iron. Iron is a very slow diffusion element ($Q_{lattice}$= 214 Jmol^{-1} [21]) and can only diffuse over short distances in the Al-lattice. However, when reaching a dislocation line or subgrain boundary, pipe diffusion

is possible, which typically lowers the activation energy by ~40%. After 92.5% deformation the mean diffusion path to a nearby pipe (dislocation) is shorter than with only 50% deformation, explaining the differences seen in Fig. 1.

The iron atoms are smaller than aluminium and dissolved iron will be attracted to lattice defects where it will lower the misfit strains. The sluggish recovery kinetics seen in both 50% and 92.5% during the first annealing step can be explained by solute drag caused by dissolved iron atoms impeding the mobility of dislocations and subgrain boundaries. In fact, the etched surfaces of annealed samples shown in Fig. 5 reveal stringers of pits (manifestation of Fe precipitation) in patterns similar to micro-shear bands and lamellar boundaries – typical features of deformed microstructures. Very few pits were located at high angle grain boundaries of recrystallized grains, refuting any theories of precipitation by sweeping of high angle grain boundaries as described by e.g. Vandermeer [17].

The softening behavior in Fig. 2 shows that the hardness drops quickly after sample A and D starts to recrystallize. In the inter-annealed samples both recovery and recrystallization is rapid. Thus, the precipitates exert only a small Zener drag force on dislocations and boundaries. The particle density was found to be very low - about 0.9 μm^{-2}. In addition, the Al_3Fe phase only had a partial coherency with the matrix which does not contribute to the strength as much as a fully coherent precipitate. The spherical morphology and partial coherence is in accordance with the observations by Davies et al.[10] and Yamamoto et al.[11].

Iron in the form of Al_3Fe and α_h-AlFeSi does not give the same strength contribution as dissolved iron. Still, in Fig. 2 a strength increase is seen for the 50% deformed samples (A, B, C) that have been inter-annealed in as-deformed state, but this is related to the Hall-Petch effect. Inter-annealing of the 50% deformed samples refines the grain size and for the 92.5% deformed samples

this effect is of course less noticeable because even without interannealing the grain size is already significantly smaller for sample D than sample A. It is possible that the grain refining effect on strength balances that of the reduced strength due to precipitation.

According to Thermo-Calc, only α-AlFeSi and β-AlFeSi should be stable at 300 °C. However, in literature mainly the metastable precursor phase Al_6Fe and the stable Al_3Fe phases are reported. It is clear from the present investigations that deformation promotes precipitation and that the Al_3Fe forms fairly easily, as no Al_6Fe was observed after annealing. However, Miki and Warlimont [22] have found Si additions to promote precipitation of Al_3Fe and can explain why no Al_6Fe is observed here as there is 0.05wt% Si in the investigated alloy.

Because the 50% deformed samples do not form a strong texture it is of more interest to focus on the 92.5% deformed samples. The texture after deformation in the two 92.5% deformed samples have the same components and with similar peak intensity. After inter-annealing, the S and, in particular, the Brass components have a higher intensity and there is a general sharpening of the texture. These differences are not expected to be of significance and in the recrystallization texture there are only minor differences in the intensity of the deformation texture components between sample D and E. However, Fig. 4 shows that the main differences are related to the Cube texture component. Cube itself becomes stronger and the RD-rotated Cube and Goss components are replaced by a TD-rotated Cube in the inter-annealed sample. The R-texture component was not detected in any of the annealed samples. Thus, precipitation of iron during inter-annealing clearly causes a stronger Cube texture component during recrystallization as iron in solution is inhibiting growth of Cube as most literature describe. That precipitates cause a Zener drag effect which suppress the Cube component during recrystallization was not observed in this work [13]. To highlight the effect of dissolved iron, a sample of the 92.5% deformed material was flash-annealed

at 500 °C for 10 seconds. The conductivity after recrystallization was only 35 m/Ωmm^2 indicating that most of the dissolved iron after homogenization was still in solution. Thus, recrystallization was strongly influenced by solute drag. The resulting texture for constant φ_2=0° and φ_2=55° is shown in Fig. 6. The Cube component, although well defined, is much weaker than in sample D and E where there is less dissolved iron for more of the softening and recrystallization process. That there is also an S-component rotated towards R is a strong confirmation of the works by Suzuki et al. [15], Marshall and Ricks[4] and Ito et al. [14] which suggested that dissolved iron promote the R component. Because there is only weak scattering of R about the S texture component, Hirsch and Lücke [23] have found this to be a sign of continuous recrystallization – which is indeed reasonable when we look at Fig. 7 where the typical β-fiber of the deformation texture is relatively strong. The resulting texture during continuous growth is typically more influenced by oriented nucleation. Hence, it seems like dissolved iron influences growth of Cube nuclei negatively during the early stages of recrystallization rather than during the later stages of grain growth similarly to what Ito et al. [11] found.

5. Conclusions

In a supersaturated state, iron in solution will cause precipitation of Al_3Fe and α_h-AlFeSi phases during annealing at 320 °C. Because iron has a low diffusivity, precipitation is promoted by increased deformation – the precipitates form on features of the deformation structure like micro-shear bands and lamellar boundaries. By subsequent deformation and annealing, softening is faster by roughly a factor 10^3 in the AA1070 alloy investigated here.

As a consequence of solute drag and concurrent precipitation during the first annealing sequence, the recrystallization texture of inter-annealed samples, where the precipitates are already

present, is strongly influenced. Dissolved iron in solution inhibits the formation of the Cube texture component, most likely in the nucleation phase of recrystallization. Instead of being RD-rotated after the first annealing step, after the second annealing step the Cube texture also has a TD-rotated component. The R texture component appears only in a flash-annealed sample with a high level of dissolved iron.

6. References

1. Belov, N.A.; Aksenov, A.A.; Eskin, D.G. *Iron in aluminium alloys - impurity and alloying element*. CRC Press Taylor&Francis Group **2002**.
2. Zhang, L.F.; Gao, J.W.; Damoah, L.N.W.; Robertson, D.G. Removal of iron from aluminum: A review. *Mineral Processing and Extractive Metallurgy Review* **2012**, *33*, 99-157.
3. Masing, G.; Lucke, K.; Nolting, P. Einfluss von Kleinen Beimengungen auf das Rekristallisationsverhalten von Reinstaluminium. *Zeitschrift Fur Metallkunde* **1956**, *47*, 64-74.
4. Marshall, G.J.; Ricks, R.A. Role of iron during recovery and recrystallization of aluminium-iron alloys. *Materials Science Forum* **1993**, *113-115*, 245-250.
5. Marshall, G.J.; Ricks, R.A.; Limbach, P.K.F. Controlling lower temperature recovery and recrystallization in commercial purity aluminum. *Materials Science and Technology* **1991**, *7*, 263-269.
6. Hasenclever, J. The important role of dissolved elements (Mn,Fe) in the process of rolled products and their effects on final properties. In *Aluminium alloys 2006, pts 1 and 2: Research through innovation and technology*, Poole, W.J.; Wells, M.A.; Lloyd, D.J., Eds. 2006; Vol. 519-521, 1447-1452.
7. Grewen, J.; Heimendahl, M.v. Gefuge, Textur und Zipelbildung von Al99,5 in Abhangigkeit von der Verformung. *Zeitschrift Fur Kristallographie* **1968**, *59*, 205-212.
8. Metzger, M.; Levy, M. Internal-friction of aluminum crystals containing iron. *Journal De Physique* **1985**, *46*, 261-264.
9. Holm, K.; Hornbogen, E. Annealing of supersaturated and deformed Al-3.042 wt percent Fe solid solutions. *Journal of Materials Science* **1970**, *5*, 655-662.
10. Davies, R.K.; Randle, V.; Marshall, G.J. Continuous recrystallization-related phenomena in a commercial Al-Fe-Si alloy. *Acta Materialia* **1998**, *46*, 6021-6032.
11. Yamamoto, A.; Kato, T.; Tsubakino, H. Precipitation in an Al-300 ppm Fe alloy. *Materials Transactions* **2004**, *45*, 3106-3113.
12. Bond, A.P.; Bolling, G.F.; Domian, H.A.; Biloni, H. Microsegregation and tendency for pitting corrosion in high-purity aluminum. *Journal of the Electrochemical Society* **1966**, *113*, 773-778.

13. Ito, K.; Musick, R.; Lucke, K. The influence of iron content and annealing temperature on the recrystallization textures of high-purity aluminum iron-alloys. *Acta Metallurgica* **1983**, *31*, 2137-2149.
14. Ito, K.; Lucke, K.; Rixen, R. Influence of pre-annealing and annealing temperatures on recrystallization textures of cold-rolled aluminum-iron alloys. *Zeitschrift Fur Metallkunde* **1976**, *67*, 338-347.
15. Suzuki, T.; Arai, K.; Shiga, M.; Nakamura, Y. Impurity effect on cube texture in pure aluminum foils. *Metallurgical Transactions a-Physical Metallurgy and Materials Science* **1985**, *16*, 27-36.
16. Ekstrom, H.E.; Hutchinson, W.B.; Oscarsson, A. The influence of iron on textures and earing in alumnium sheet. *Key Engineering Materials* **1990**, *44-45*, 188-210.
17. Vandermeer, R.A. A transient effect in grain-boundary migration during recrystallization in aluminium. *Acta Metallurgica* **1967**, *15*, 447-458.
18. Black, P.J. The structure of FeAl3 .1. *Acta Crystallographica* **1955**, *8*, 43-48.
19. Mondolfo, L.F. *Aluminium alloys: Structure and properties*. Butterworths: London, 1976.
20. Kubota, S.; Kawai, M.; Yamamoto, M.; Shiga, M. Effects of cold rolling and heat treatments on Fe precipitation in high purity alloys studied by Mossbauer spectroscopy. *Journal of Japan Institute of Light Metals* **2001**, *51*, 635-639.
21. Du, Y.; Chang, Y.A.; Huang, B.Y.; Gong, W.P.; Jin, Z.P.; Xu, H.H.; Yuan, Z.H.; Liu, Y.; He, Y.H.; Xie, F.Y. Diffusion coefficients of some solutes in fcc and liquid Al: Critical evaluation and correlation. *Mater. Sci. Eng. A-Struct. Mater. Prop. Microstruct. Process.* **2003**, *363*, 140-151.
22. Miki, I.; Warlimont, H. Morphologie and Wachstumskinetic der Ausscheidungen in Aluminiumreichen Aluminium-Eisen und Aluminium-Eisen-Silizium-legierungen. *Zeitschrift Fur Metallkunde* **1968**, *59*, 254-264.
23. Hirsch, J.; Lucke, K. The application of quantitative texture analysis for investigating continuous and discontinuous recrystallization processes of Al-0.01Fe. *Acta Metallurgica* **1985**, *33*, 1927-1938.

Figure captions

Figure 1. Electrical conductivity as a function of time. 10^0s corresponds to the as-deformed state. (a) Material A, B and C, (b) Material D and E.

Figure 2. Evolution in hardness in annealed samples with time. 10^0 s refers to as-deformed state. (a) Material A, B and C, (b) Material D and E.

Figure 3. Typical TEM micrograph and corresponding EDS spectra from samples deformed 50% and 92.5% and directly annealed for 10^4 and 10^5 seconds. (a) TEM bright field image of Al_3Fe (1) and α_h-AlFeSi (2) phases precipitating during annealing. (b) EDS spectra from particles small spherical particles labelled "1" (upper) and from the larger elongated particle labelled "2" (lower) in (a).

Figure 4. Annealing textures in the form of ODFs shown for the constant φ_2=0° section only.

Figure 5. SEM images of etch pits (black/dark colored dots) at iron-precipitates along micro shear bands and lamellar boundaries in 50% (a) and 92.5% (b) deformed samples after annealing, respectively.

Figure 6. Recrystallization texture (ODF; φ_2 = 0° and 55° sections, respectively) of a sample deformed 92.5% after homogenization and then flash-annealed at 500 °C for 10 seconds.

Figure 7. Recrystallizations texture in the form of cube texture intensity (bars) and β-fibre intensity) of 92.5% deformed samples after different types of annealing.

Table captions

Table 1 Samples and processing

Figures

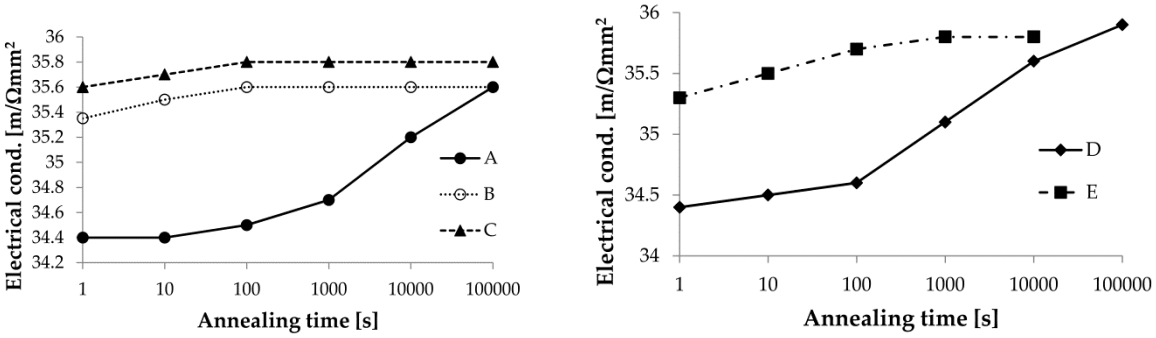

a b

Figure 1. Electrical conductivity as a function of time. 10^0s corresponds to the as-deformed state. (a) Material A, B and C, (b) Material D and E.

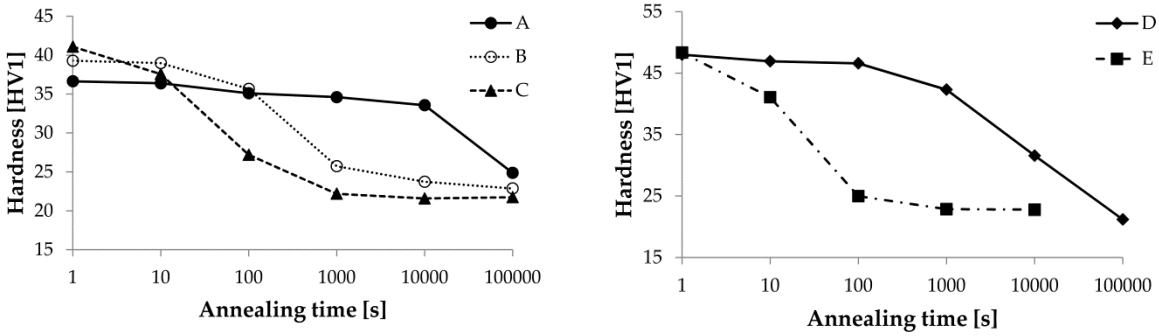

a b

Figure 2. Evolution in hardness in annealed samples with time. 10^0 s refers to as-deformed state.

(a) Material A, B and C, (b) Material D and E.

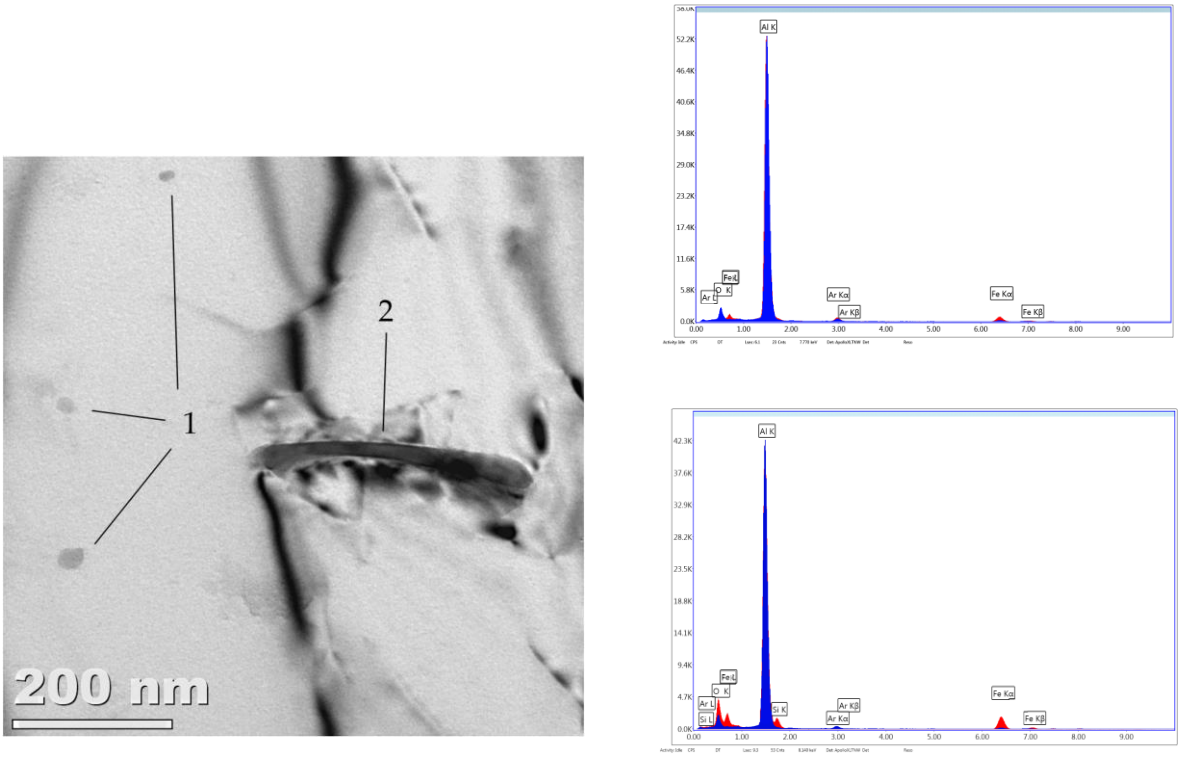

a b

Figure 3. Typical TEM micrograph and corresponding EDS spectra from samples deformed 50% and 92.5% and directly annealed for 10^4 and 10^5 seconds. (a) TEM bright field image of Al_3Fe (1) and α_h-AlFeSi (2) phases precipitating during annealing. (b) EDS spectra from particles small spherical particles labelled "1" (upper) and from the larger elongated particle labelled "2" (lower) in (a).

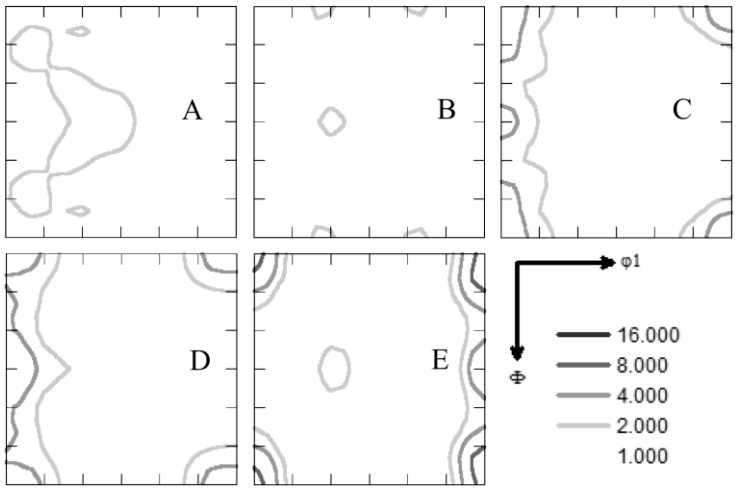

Figure 4. Annealing textures in the form of ODFs shown for the constant φ_2=0° section only.

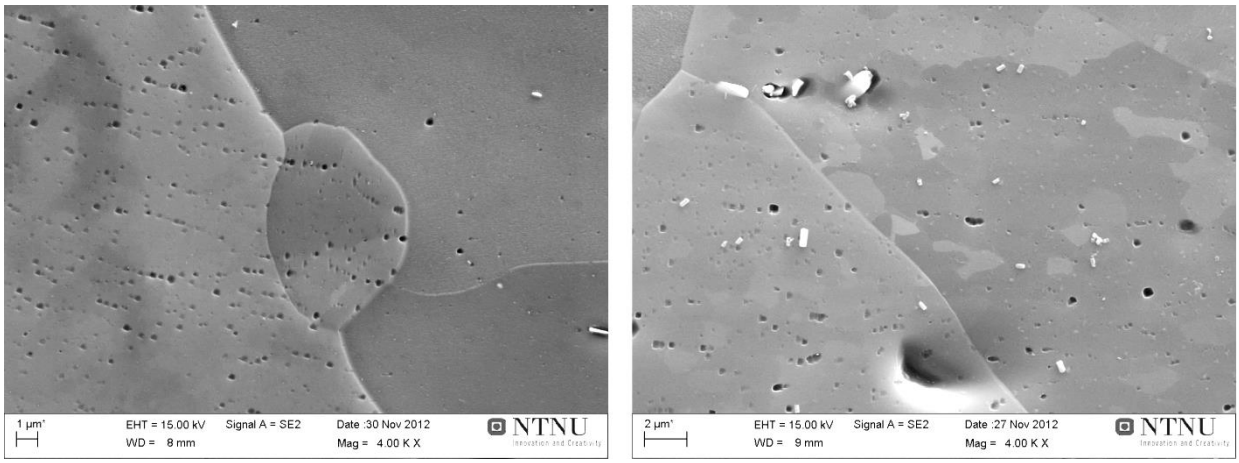

(a) (b)

Figure 5. SEM images of etch pits (black/dark colored dots) at iron-precipitates along micro shear bands and lamellar boundaries in 50% (a) and 92.5% (b) deformed samples after annealing, respectively.

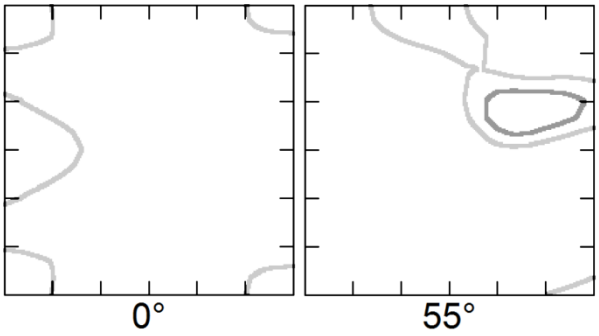

Figure 6. Recrystallization texture (ODF; φ_2 = 0º and 55º sections, respectively) of a sample deformed 92.5% after homogenization and then flash-annealed at 500 °C for 10 seconds.

.

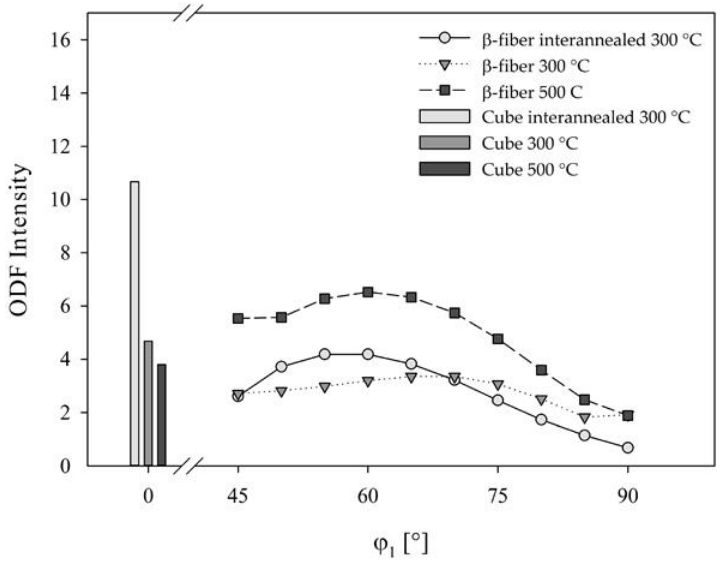

Figure 7. Recrystallizations texture in the form of cube texture intensity (bars) and β-fibre intensity) of 92.5% deformed samples after different types of annealing.

Tables

Table 1 Samples and processing

Sample	Processing	Final annealing temperature
A	def. 50%	320 °C
B	def. 50% + 10^5 s/320 °C + def. 50%	320 °C
C	def. 92.5% + 10^5 s/320 °C + def. 50%	320 °C
D	def. 92.5%	300 °C
E	def. 50% + 10^5 s/320 °C + def. 92.5%	300 °C